Available online at www.sciencedirect.com
SCIENCE DIRECT®
Journal of Hydrology 286 (2004) 249–270
Journal of Hydrology
www.elsevier.com/locate/jhydrol

Terrestrial vegetation and water balance—hydrological evaluation of a dynamic global vegetation model

Dieter Gerten[a,*], Sibyll Schaphoff[a], Uwe Haberlandt[b], Wolfgang Lucht[a], Stephen Sitch[a]

[a]*Department of Global Change and Natural Systems, Potsdam Institute for Climate Impact Research, Telegrafenberg C4, D-14412 Potsdam, Germany*
[b]*Institute for Hydrology, Water Management and Environmental Engineering, Ruhr-Universität, Universitätsstrasse 150, D-44780 Bochum, Germany*

Received 27 March 2003; revised 2 September 2003; accepted 26 September 2003

Abstract

Earth's vegetation plays a pivotal role in the global water balance. Hence, there is a need to model dynamic interactions and feedbacks between the terrestrial biosphere and the water cycle. Here, the hydrological performance of the Lund–Potsdam–Jena model (LPJ), a prominent dynamic global vegetation model, is evaluated. Models of this type simulate the coupled terrestrial carbon and water cycle, thus they are well suited for investigating biosphere–hydrosphere interactions over large domains. We demonstrate that runoff and evapotranspiration computed by LPJ agree well with respective results from state-of-the-art global hydrological models, while in some regions, runoff is significantly over- or underestimated compared to observations. The direction and magnitude of these biases is largely similar to those from other macro-scale models, rather than specific to LPJ. They are attributable primarily to uncertainties in the climate input data, and to human interventions not considered by the model (e.g. water withdrawal, land cover conversions). Additional model development is required to perform integrated assessments of water exchanges among the biosphere, the hydrosphere, and the anthroposphere. Yet, the LPJ model can now be used to study inter-relations between the world's major vegetation types and the terrestrial water balance. As an example, it is shown that a doubling of atmospheric CO_2 content alone would result in pronounced changes in evapotranspiration and runoff for many parts of the world. Although significant, these changes would remain unseen by stand-alone hydrological models, thereby emphasizing the importance of simulating the coupled carbon and water cycle.

Keywords: Macro-scale models; Global hydrology; Runoff; Transpiration; Vegetation; CO_2 effect

1. Introduction

Vegetation and the water cycle are intrinsically coupled (Hutjes et al., 1998; Kucharik et al., 2000; Arora, 2002). Site water balance is a key determinant for the distribution (Stephenson, 1990) and productivity (Churkina et al., 1999) of terrestrial vegetation around the globe. In turn, the composition and distribution of plant communities are of fundamental importance for evapotranspiration and runoff generation (e.g. Dunn and Mackay, 1995). Plants exert considerable effects on runoff via features such as albedo and interception (Eckhardt et al.,

* Corresponding author. Fax: +49-331-288-2640.
E-mail address: dieter.gerten@pik-potsdam.de (D. Gerten).

0022-1694/$ - see front matter © 2003 Elsevier B.V. All rights reserved.
doi:10.1016/j.jhydrol.2003.09.029

2003), stomatal behaviour and transpiration (e.g. Skiles and Hanson, 1994), rooting strategy (Milly, 1997), leaf area (Neilson, 1995; Kergoat, 1998), and phenology (Peel et al., 2001). It is well-known, for example, that a reduction in forest cover increases runoff by decreasing evapotranspiration, whereas reforestation usually lowers runoff (Bosch and Hewlett, 1982).

Effects of vegetation on the hydrological cycle can also be seen at the global scale. For example, differences in the variability of annual runoff among continents are controlled not only by differences in precipitation amount but also by the geographical distribution of evergreen and deciduous vegetation (Peel et al., 2001). Additionally, the level of atmospheric CO_2 content influences regional and large-scale evapotranspiration and runoff generation by influencing the water use efficiency of plants (Wigley and Jones, 1985; Loukas and Quick, 1999). At elevated CO_2 concentrations, carbon uptake by plants and, thus, photosynthesis rate and vegetation productivity are usually higher per unit of water transpired, while conductance of water through the stomata may be smaller. Experimental evidence suggests that stomatal conductance may decrease by up to 30–40% at $2 \times CO_2$ (e.g. Eamus and Jarvis, 1989), since plants tend to reduce stomata opening to maintain an optimal balance between water loss and CO_2 absorption (Lockwood, 1999). Cramer et al. (2001) provided an example for this effect on the global scale. The vegetation models used in their study projected a notable increase in global runoff as a net effect of climate change and the fertilization effect of CO_2. This change in runoff could not be explained by increased precipitation alone, but was also driven by decreased stomatal conductance and alterations in vegetation composition and distribution (Cramer et al., 2001). There is an ongoing debate on the extent to which non-linear vegetation responses and land–atmosphere feedbacks, such as increased primary production, higher leaf temperatures, and seasonal changes in soil moisture, counteract the antitranspirant effect (e.g. Kimball et al., 1999).

Global water resources and runoff from large river basins can now be more or less realistically simulated by macro-scale hydrological models (Arnell, 1999a,b; Fekete et al., 2002; Alcamo et al., 2000; Vörösmarty et al., 2000; Döll et al., 2003). However, parameterisation of vegetation is insufficient in these models, and the inter-play between vegetation and water is not described in a process-based manner. Therefore, important biosphere–hydrosphere interactions, and particularly their temporal dynamics, may be neglected by stand-alone hydrological models. For instance, they cannot capture sufficiently hydrological effects resulting from changes in vegetation composition and distribution. Such effects, however, are likely to occur in response to climate change (Gitay et al., 2001), and therefore have been considered in climate change impact studies by use of equilibrium biogeography models (Neilson et al., 1998).

Thus, realistic assessment of spatio-temporal variability in the terrestrial water budget requires models that mechanistically link vegetation dynamics and hydrological processes. Among candidate models to meet this requirement are land surface schemes used in climate models, but they also do not simulate transient changes in vegetation structure and distribution (e.g. Levis et al., 1996; Nijssen et al., 2001). In addition, the computed water balance usually is less reliable than those from explicit hydrological models (see Döll et al., 2003). Alternative candidates are equilibrium and dynamic global vegetation models (DGVMs). The latter are able to simulate transient structural changes in Earth's major vegetation types in response to variations in, among other factors, climate, water availability, and atmospheric CO_2 content. This is ensured, for instance, via explicitly describing the coupling between photosynthetic demand for CO_2 and water loss through the stomata (for an overview, see Churkina et al., 1999). DGVMs, thus, are well suited tools for the assessment of hydrological consequences arising out of environmental change at large scales. But, they require thorough validation of the embodied water balance. The hydrological output of some global vegetation models have been tested recently (Neilson, 1995; Foley et al., 1996; Kucharik et al., 2000). However, it remains unclear how well these models reproduce runoff at the scale of single basins, and to what extent these estimates deviate from those of stand-alone hydrological models. Problems in the hydrological performance of global vegetation models and potential ways to overcome

such shortcomings have not been specified so far (but see Lenters et al., 2000; Foley et al., 2002 for regional applications).

The present study provides a hydrological evaluation of a leading DGVM, the Lund–Potsdam–Jena model (hereafter LPJ; Sitch et al., 2003). The scope is to identify shortcomings in runoff estimation by an uncalibrated DGVM, and potential advantages over hydrological models. Therefore, simulated long-term mean annual runoff was compared with observations from over 600 macro-scale river basins around the world. Inter-annual and seasonal runoff dynamics were explored in more detail for a subset of these basins. To assess the performance of the LPJ-DGVM relative to stand-alone global hydrological models, simulated continental runoff fields were compared with those replicated by three state-of-the-art models of that type. Additionally, simulated evapotranspiration was validated against, respectively, large-scale estimates and stand-level observations from a range of sites across Europe.

To provide an idea to what extent terrestrial vegetation affects the large-scale water balance, the model was run under a hypothetic CO_2-doubling scenario without assuming climatic changes. The resulting spatial patterns of change in runoff and evapotranspiration compared to the standard run were analysed.

2. The Lund–Potsdam–Jena model

Lund–Potsdam–Jena (LPJ) is a coupled non-equilibrium biogeography–biogeochemistry model, which combines process-based representations of terrestrial vegetation dynamics and land–atmosphere carbon and water exchanges in a modular framework (Fig. 1). Since it is described in detail elsewhere (Sitch et al., 2003), only a short overview will be provided here. LPJ explicitly considers key ecosystem processes such as vegetation growth, mortality, carbon allocation, and resource competition, though their representation is of intermediate complexity to allow for global applications. To account for the variety of structure and functioning among plants, 10 plant functional types (PFTs) are distinguished (Table 1). Leaf phenology of summergreen and raingreen PFTs is determined daily, depending on temperature and water stress thresholds. Gross primary production is computed based on a coupled photosynthesis–water balance scheme; net primary production is given by subtracting autotrophic respiration. After additional subtraction of a reproduction cost, the remaining carbon is allocated to three pools for producing new tissue. Carbon from dead leaves and roots enters litter; decomposition of litter and soil organic matter is driven by soil temperature and water content. A PFT-specific mortality rate is determined at the end of each year as a result of heat stress, low growth efficiency, a negative carbon balance, light competition, or violation of bioclimatic limits. The presence and fractional coverage of PFTs is thus determined annually according to individual bioclimatic, physiological, morphological, and fire-resistance features (Sitch et al., 2003). The structure and distribution of the PFTs is decisive for the simulated site water balance, since evapotranspiration, soil water content, and runoff generation are modulated by PFT-specific attributes such as interception storage capacity, seasonal phenology, rooting depth, and photosynthetic activity.

Overall, LPJ simulates well the global terrestrial carbon pool sizes and fluxes, and captures the biogeographical distribution of Earth's major biomes (Sitch et al., 2003). Recent applications of the model include assessments of the carbon balance of the terrestrial biosphere (Prentice et al., 2000; Cramer et al., 2001; McGuire et al., 2001), the representation of fire regimes (Venevsky et al., 2002), and the simulation of transient vegetation responses to climate warming (Joos et al., 2001; Lucht et al., 2002).

The version of LPJ presented here incorporates an improved representation of the water cycle compared to the model described in Sitch et al. (2003). The most important changes encompass the inclusion of additional processes such as interception and soil evaporation, and the stochastic distribution of precipitation (Fig. 1). A few PFT parameters had to be re-adjusted to ensure realistic simulation of vegetation features and the carbon balance after these modifications. A detailed description of the water balance computations is given in the following sections.

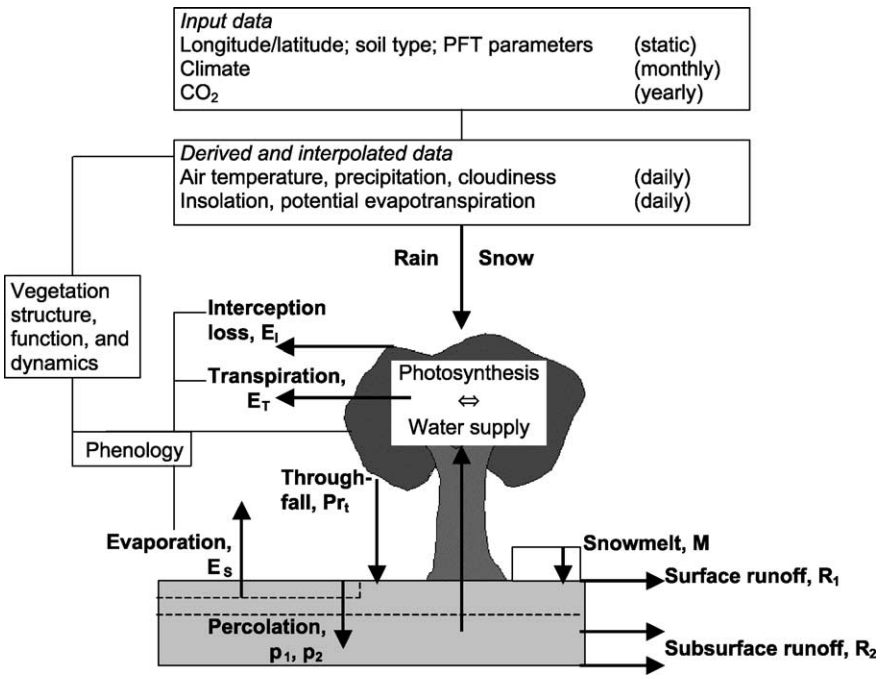

Fig. 1. Schematic representation of the water balance computed for each grid cell by the dynamic global vegetation model LPJ. The thick arrows indicate water fluxes; the abbreviations of these fluxes are defined in the text.

2.1. Potential evapotranspiration

Daily equilibrium evapotranspiration rate (E_q, in mm d^{-1}) at the regional scale depends primarily on net radiation and temperature, and is given by

$$E_q = [\Delta/(\Delta + \gamma)]R_n/L \quad (1)$$

where R_n (J m^{-2} d^{-1}) is net radiation (net short-wave flux minus net long-wave flux) calculated from latitude, day of the year, sunshine hours and air temperature following a standard approach (for further detail, see Prentice et al., 1993). Δ is the rate of increase of the saturation vapour pressure with temperature, γ the psychrometer constant

Table 1
Hydrologically relevant PFT parameter values

Plant functional type (unit)	E_{max} (mm d^{-1})	i	g_{min} (mm s^{-1})	SD_{min}	z_1	z_2
Tropical broadleaved evergreen tree	7.0	0.02	0.5	0.0	0.85	0.15
Tropical broadleaved raingreen tree	7.0	0.02	0.5	0.1	0.60	0.40
Temperate needleleaved evergreen tree	5.0	0.06	0.3	0.0	0.70	0.30
Temperate broadleaved evergreen tree	5.0	0.02	0.5	0.0	0.70	0.30
Temperate broadleaved summergreen tree	5.0	0.02	0.5	0.0	0.70	0.30
Boreal needleleaved evergreen tree	5.0	0.06	0.3	0.0	0.90	0.10
Boreal needleleaved summergreen tree	5.0	0.06	0.3	0.0	0.90	0.10
Boreal broadleaved summergreen tree	5.0	0.06	0.5	0.0	0.90	0.10
C3 perennial grass	5.0	0.01	0.5	0.2	0.80	0.20
C4 perennial grass	7.0	0.01	0.5	0.1	0.80	0.20

E_{max}, maximum transpiration rate; i, coefficient for calculation of interception; g_{min}, minimum canopy conductance; SD_{min}, ratio between water supply and demand below which stomata close; z_1, fraction of roots in the upper soil layer; z_2, dto., lower soil layer.

(~ 65 Pa K^{-1}), and L the latent heat of vaporization of water ($\sim 2.5 \times 10^6$ J kg^{-1}). Potential evapotranspiration is determined by multiplying E_q with the Priestley–Taylor coefficient, α (Priestley and Taylor, 1972). We assume $\alpha = 1.32$, a value that Hobbins et al. (2001) have re-examined for large-scale applications; computation of plant transpiration requires an upper limit for α (see below).

2.2. Actual evapotranspiration

Actual evapotranspiration is the sum of (a) interception loss and (b) plant transpiration for all PFTs, plus (c) evaporation from bare soil, calculated as follows.

2.2.1. Interception loss

Canopy storage capacity (S_I, mm d^{-1}) is defined as a function of biome, leaf area index (LAI), and precipitation amount (Pr, mm d^{-1}), following the approach of Kergoat (1998)

$$S_I = \mathrm{Pr} \times \mathrm{LAI} \times i \times f_V \quad (2)$$

where f_V denotes the fraction of the grid cell covered by vegetation, taking account of daily phenology. The factor i is a dimensionless biome-dependent proxy for the rainfall regime (Table 1). Storage capacity is relatively high in boreal forests, and lower in tropical forests due to high rainfall intensity. Also, i is lower for grasslands than for forests (Kelliher et al., 1993). Precipitation is differentiated between rain and snow depending on whether daily mean air temperature is above or below 0 °C. All precipitation on days with negative mean temperature adds to snowpack; we do not distinguish between interception of rain and snow. Daily interception loss (E_I) is then given by

$$E_I = E_q \alpha w \quad (3)$$

where w represents the fraction of day-time that the canopy is wet, defined as follows (Kergoat, 1998):

$$w = \mathrm{Min}(S_I/[E_q \alpha], 1) \quad (4)$$

Night-time fluxes are neglected; the remaining day-time canopy-available energy (1-w) is used for plant transpiration.

2.2.2. Transpiration

Transpiration is modelled as the lesser of an atmosphere-controlled demand function (D) and a plant-controlled supply function (S), as proposed by Federer (1982):

$$E_T = \mathrm{Min}(S, D) f_V \quad (5)$$

Transpirational supply is determined by the maximum transpiration rate that can be sustained under well-watered conditions (E_{max}), and declines linearly with relative soil moisture (wr)

$$S = E_{max}\,\mathrm{wr} \quad (6)$$

E_{max} should exhibit minor differences among vegetation types, and is assigned a value of 5–7 mm d^{-1} (e.g. Kelliher et al., 1993; Table 1). wr gives the ratio between current soil water content and plant-available water capacity (w_{max}, the texture-dependent difference between field capacity and wilting point). The soil is treated as a simple bucket consisting of two layers with fixed thickness (upper [d_1], 0.5 m; lower [d_2], 1.0 m). A third layer representing the top 0.2 m is distinguished to calculate soil evaporation (see below). The wr ratio is computed for both soil layers by weighting their relative soil water contents (w_1, w_2; see below) with the fraction of roots present in the respective layer (z_1, z_2; Table 1).

Atmospheric demand represents ›unstressed transpiration‹ (Federer, 1982), which occurs when stomatal opening is not limited by reduced water potential in the plant. Following Monteith (1995), daily demand is a hyperbolic function of canopy conductance (the sum of stomatal conductance of all leaves for a given PFT):

$$D = (1 - w) E_q \alpha_m / (1 + g_m/g_{pot}) \quad (7)$$

Following Huntingford and Monteith (1998), a maximum Priestley–Taylor coefficient, $\alpha_m = 1.391$, and a scaling conductance, $g_m = 3.26$ mm s^{-1}, is defined. Demand approximates $E_q \alpha_m$ when the canopy is dry and g_{pot}—the potential canopy conductance that can be achieved when there is no water limitation—tends to infinity. g_{pot} (mm s^{-1}) is directly related to the photosynthesis rate as follows (details in Haxeltine and Prentice, 1996;

Sitch et al., 2003):

$$g_{pot} = g_{min} + 1.6A_{dt}/[c_a(1-\lambda)] \quad (8)$$

Here, g_{min} is a PFT-specific minimum canopy conductance (Table 1) that accounts for plant water loss not directly linked to photosynthesis (e.g. guttation). A_{dt} is daytime net photosynthesis (g C d^{-1} m^{-2}); c_a is ambient CO_2 (mole fraction). λ is the stomata-controlled ratio between intercellular and ambient CO_2 partial pressure in the absence of water limitation; it is lower for warm-zone C4 grasses (0.4) than for C3 plants, i.e. trees and cool-zone grasses (0.8). Thus, at high CO_2 concentrations, plants increase their water use efficiency by transpiring less water per unit of carbon fixed (Lockwood, 1999). The coupled modelling of photosynthesis and transpiration accounts for the capacity of plants to balance water loss and CO_2 assimilation at varying CO_2 levels (see Section 1). Furthermore, actual canopy conductance is computed to fall below g_{pot} if $S < D$. Decreasing water availability thus limits simultaneously both the transpiration rate and the photosynthesis rate. It is assumed that stomata close completely when the ratio of S over D reaches a threshold value (SD_{min}, Table 1).

2.2.3. Soil evaporation

Daily evaporation from bare soil (E_S) occurs at the simulated fraction of the grid cell ($1 - f_V$) not covered by vegetation (determined annually), which may extend towards the plant-covered area according to the daily status of PFT-specific leaf phenology (see Fig. 1). Evaporation declines linearly as the soil dries, a simple approach that is suitable for large scales (Huang et al., 1996)

$$E_S = E_q \alpha wr_{20}(1 - f_V) \quad (9)$$

where wr_{20} represents the relative moisture in the upper 20 cm of the soil column, which is updated daily by Pr and E_S. E_T from this layer, and percolation, are determined as a fraction of the respective values for the upper soil layer (d_1). E_T is weighted by a factor of 1.3 (derived from Jackson et al., 1996), as more roots can be expected in the upper 20 cm than below. Capillary rise from groundwater is not taken into account due to the lack of global data on the height of the groundwater table.

2.3. Soil water storage and runoff generation

Water content of both soil layers is updated daily taking account of snowmelt (M), throughfall ($Pr_t = Pr - E_I$), transpiration, evaporation, percolation through the layers, and runoff:

$$\Delta w_1 = (Pr_t + M - \beta_1 \times E_T - E_S - p_1 - R_1)/(w_{max} d_1) \quad (10)$$

$$\Delta w_2 = (p_1 - \beta_2 \times E_T - R_2 - p_2)/(w_{max} d_2) \quad (11)$$

Here, Δw_1 and Δw_2 are daily changes in soil water content of both layers (expressed as a fraction of the respective w_{max}); β_1 and β_2 represent the fractions of water extracted for transpiration from each layer (such that $\beta_1 + \beta_2 = 1$). Snowmelt (mm d^{-1}) is computed using a degree–day method (Choudhury et al., 1998)

$$M = (1.5 + 0.007Pr)T_a \quad (12)$$

where T_a is air temperature above 0 °C. Percolation rate from the upper to the lower soil layer (p_1, mm d^{-1}) depends on soil texture and layer thickness, and declines exponentially with soil moisture

$$p_{1,2} = k w_1^2 \quad (13)$$

where k is the texture-dependent conductivity, varying from 5.0 mm d^{-1} for sandy soils to 0.2 mm d^{-1} for vertisols. The model diagnoses surface runoff (R_1) and subsurface runoff (R_2) from the excess of water over field capacity of the upper and the lower soil layer, respectively. In addition, the amount of water percolating through the second soil layer is assumed to contribute to subsurface runoff (p_2, mm d^{-1}). The sum of the three runoff components ($R_1 + R_2 + p_2$) is used for validation. There is no lateral redistribution of water among grid cells, and no routing in the stream network.

3. Data and methods

3.1. Model input

The LPJ model was run for the period 1901–1998, preceded by a 1000-year spinup period

to reach an initial equilibrium with respect to carbon pools and vegetation cover (see Sitch et al., 2003). The simulations were driven by gridded monthly fields (0.5° resolution) of air temperature, precipitation, number of wet days, and cloud cover from the CRU05 database (provided by the Climate Research Unit, University of East Anglia; New et al., 2000), and by texture for nine soil types (Zobler, 1986; FAO, 1991; details on soil parameterisation in Sitch et al., 2003). Non-gridded model inputs include annual CO_2 concentrations (one global value) derived from ice-core measurements and atmospheric observations, provided by the Carbon Cycle Model Linkage Project (McGuire et al., 2001). Furthermore, various parameters are assigned to the different PFTs (Sitch et al., 2003; Table 1). Cloud cover data are not available for 1997/98, so the monthly means of the previous 30 years are used for this period. Daily air temperature and cloud cover are disaggregated by linear interpolation of the monthly values. The cloud cover data are scaled to generate daily fields of sunshine hours, on which the calculation of short-wave radiation is based. Daily precipitation is disaggregated using a stochastic weather generator. Precipitation occurrence is simulated based on a first order Markov chain, using the fraction of wet days per month and transition probabilities from Geng et al., 1986. Precipitation amount on wet days is determined using an exponential distribution. Data are not adjusted for potential measurement biases, since no convincing global data set on precipitation correction factors is available (see Döll et al., 2003).

3.2. Data for validation

Simulated runoff was compared with (i) global and zonal estimates from various sources (Baumgartner and Reichel, 1975; Shiklomanov, 1997; Cogley, 1998), (ii) long-term observed mean annual runoff from 663 basins with an area $>10^4$ km^2 and an observation period >10 years (Fekete et al., 1999), and (iii) annual and monthly time series of observations for eight large river basins ($>8\times10^5$ km^2) selected to represent a range of climatic conditions and hydrological regimes (RivDIS database, Vörösmarty et al., 1996). The runoff data from Cogley (1998) are map-derived values (mainly from Korzun et al., 1978) gridded to a 1° resolution. Additionally, simulated monthly runoff was verified at the continental scale using aggregated observations from Fekete et al. (1999) and respective results from three state-of-the-art global hydrological models (WBM, Vörösmarty et al., 1998; Fekete et al., 1999; Macro-PDM, Arnell, 1999a; Nigel Arnell, pers. comm.; WaterGAP, Alcamo et al., 2000; Petra Döll, pers. comm.). As it is not our scope to discuss differences among the latter, their individual results are not identified. It should be noted that the above-mentioned hydrological models differ in various aspects from LPJ. For instance, they are based on prescribed vegetation from diverse sources, and plant transpiration is not explicitly modelled. Furthermore, runoff is routed among cells in WBM and WaterGAP, and subsurface flow is delayed within the cells in Macro-PDM, while LPJ does not consider any time-lag. All models—except for WBM—are driven by the same climatic input (CRU database), but Macro-PDM uses precipitation data corrected for potential measurement errors (Arnell, 1999a). Note that human water consumption, as described in Döll et al. (2003), is not taken into account in the runoff data from WaterGAP used here.

Simulated actual evapotranspiration was validated against (i) latitudinal estimates documented in the literature (Baumgartner and Reichel, 1975; Henning, 1989), and (ii) stand-level observations from various forest sites across Europe (data from the EUROFLUX project; Valentini, 2003). The latter were compared with total evapotranspiration computed for the grid cell in which the sites are located, without adjustment to local conditions. Note that the observed data were multiplied by a factor of 1.2 to account for an average underestimation of 20% (Wilson et al., 2002). Simulated soil moisture fields are not discussed here. However, there is strong evidence that LPJ well reproduces seasonal and inter-annual variability in near-surface soil moisture, as our results largely agree with a global, multi-annual soil moisture data set derived from spaceborne microwave measurements (Wagner et al., 2003). Moreover, Sitch et al. (2003) found good agreement between modelled and observed monthly soil water content for a number of sites in Europe and Asia, although with a former version of LPJ.

3.3. Validation methods

The quality of runoff simulations was determined by Willmott's (1982) index of agreement (A) and the mean bias error (B) (Eq. (14)). B indicates the mean absolute deviation between predicted (P_i) and observed values (O_i). The standardized A-index describes the modelling quality with respect to the variance and the mean of the observations. $A = 0$ indicates complete disagreement between P and O, while $A = 1$ indicates complete agreement (Willmott, 1982):

$$A = 1 - \left[\sum (P_i - O_i)^2 / \sum (|P_i - \bar{O}| + |O_i - \bar{O}|)^2\right] \quad (14a)$$

$$B = \frac{\sum_i (P_i - O_i)}{n} \quad (14b)$$

3.4. 2 × CO_2 simulation experiment

To explore specific contributions of DGVMs to global hydrological assessments in view of climate change, and to examine potential influences of vegetation on macro-scale runoff and evapotranspiration, an alternative model run was performed. Only the atmospheric CO_2 content was changed in this model setup, in that the input values of CO_2 concentration were doubled for each year of the historical period under consideration, including the spinup. As noted above, transpiration through the stomata should decrease under this scenario as a consequence of increased water use efficiency. Furthermore, vegetation is expected to be more productive, which may counteract the water savings due to decreased transpiration. In turn, the changes in transpiration rate, vegetation structure and production should feed back to soil water content and runoff generation. Since LPJ computes the dynamic relations among these processes, the net effect of increased atmospheric CO_2 concentration and of associated transient vegetation changes on the water balance can be quantified. Changes in annual runoff, transpiration, evaporation, and interception under the CO_2-doubling scenario were assessed for each grid cell by the two-tailed Mann–Whitney test. The test indicates whether the components of the water balance simulated with the alternative model setup differ significantly ($p < 0.05$) from the respective values calculated in the standard model run.

4. Results of model validation

Annual means of runoff and evapotranspiration computed by LPJ lie well within the range of other estimates around the world (Figs. 2 and 3; Table 2). Simulated individual components of annual evapotranspiration—transpiration, interception, and evaporation—are also in good agreement with respective estimates from biosphere models (Levis et al., 1996; Choudhury et al., 1998; data not shown). The general quality of the LPJ simulations agrees very well with that of state-of-the-art global hydrological models (Table 3, upper panel). Three zones can roughly be distinguished with respect to simulation quality of annual runoff (Fig. 2). (i) Model results are good for the temperate regions and large parts of Central Asia and North America. (ii) Overestimations occur in semi-arid and arid regions, particularly in northern Africa, parts of South America, and India. (iii) Underestimations are frequent particularly in subarctic regions. Seasonal hydrographs simulated by LPJ are also in general accordance with results from global hydrological models (Fig. 4). However, notable deviations between observed and predicted runoff occur at times in certain regions. Specifically, LPJ as well as the three hydrological models overestimate year-round runoff in Africa, and temporally in Australia. Moreover, the hydrographs generally appear to be advanced by several weeks especially in South America, but also during spring in Europe, Asia, and North America (Fig. 4).

This large-scale pattern reflects the variable model performance at the scale of single river basins (Figs. 5 and 6; Table 3), and at the stand-level, respectively (Fig. 7). LPJ reproduces well inter- and intra-annual runoff variations for rivers such as the Danube and the Mississippi. Analogously, simulated evapotranspiration is in surprisingly good agreement with observations for a range of sites across Europe, considering that no adjustment with respect to local climate and soil properties was made for the calculations (Fig. 7). While annual runoff of

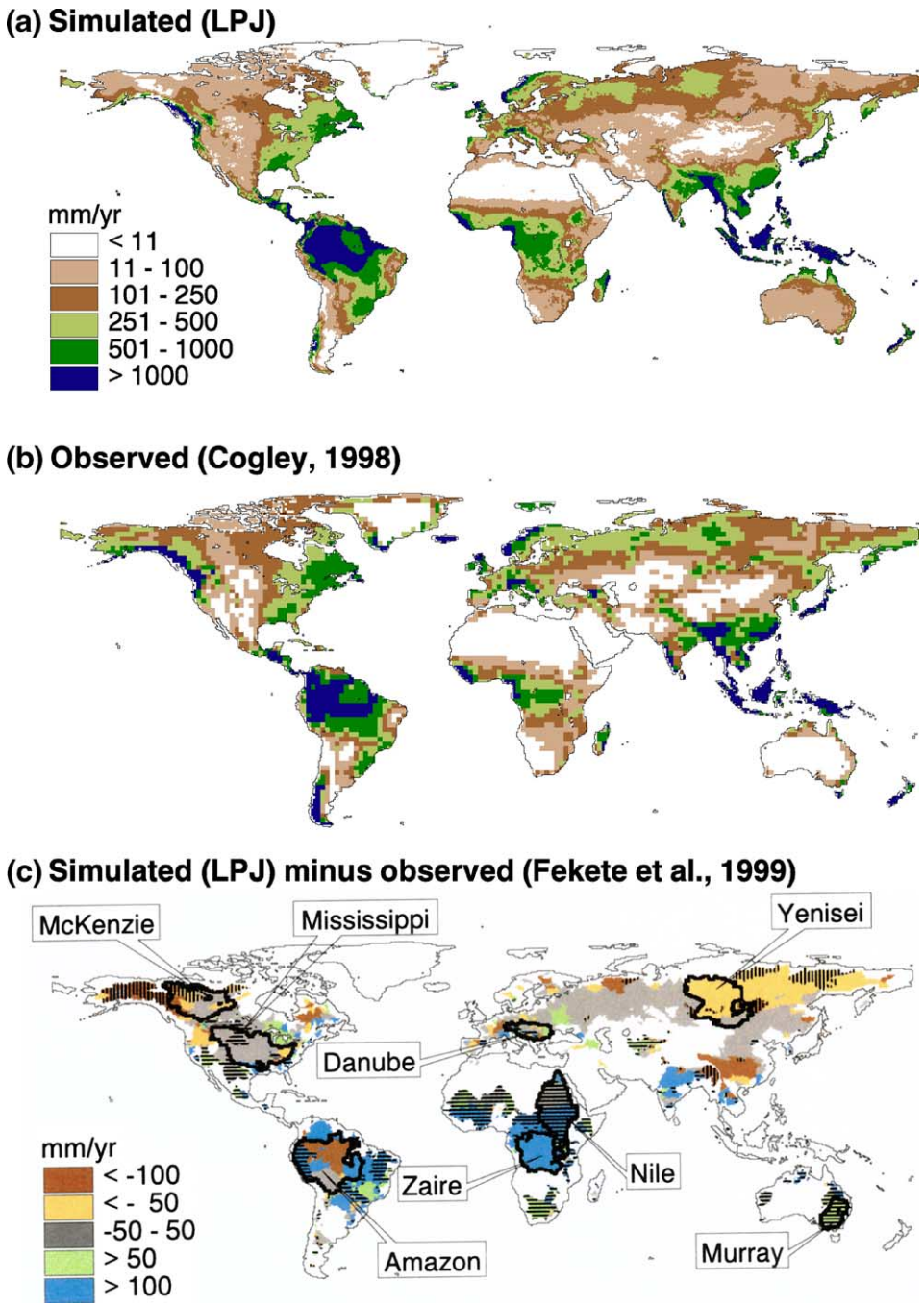

Fig. 2. Long-term annual means (mm) of runoff: (a) LPJ simulations for the period 1961–1990. (b) Observations from Cogley (1998) for diverse time periods. (c) Differences (mm) between simulated and measured runoff for 663 basins, based on time periods with different lengths (Fekete et al., 1999). Hatched areas indicate basins where simulated runoff is $<50\%$ (vertical lines), and $>200\%$ of observed discharge, respectively (horizontal lines; including basins with negative runoff in Fekete et al., 1999). Time series for the indicated individual basins are presented in Figs. 5 and 6.

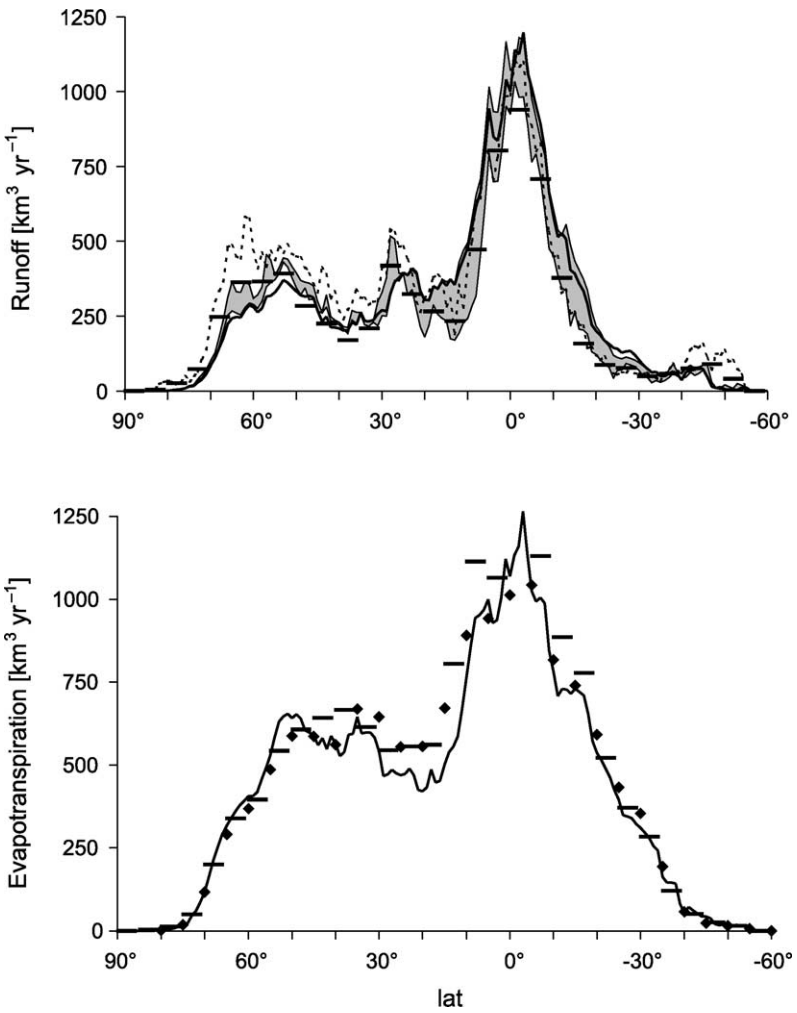

Fig. 3. Estimates of long-term annual means of (a) runoff (km^3), (b) total evapotranspiration from land (km^3), aggregated into 1° or 5° latitude zones. The thick straight line represents the LPJ simulations. The black horizontal bars refer to estimates based on observed precipitation and runoff (Baumgartner and Reichel, 1975). The shaded area in (a) gives the range of estimates from the three macro-scale hydrological models, Macro-PDM, WBM, and WaterGAP; the dotted line refers to observations from Cogley (1998). The diamonds in (b) represent the evapotranspiration calculated by Henning (1989).

Table 2
Global estimates of average annual runoff from land (km^3), excluding Antarctica

Source	LPJ-DGVM	Model 1	Model 2	Model 3
Runoff (km^3)	40,143	38,928	35,332	44,795
Source		Baumgartner and Reichel (1975)	Shiklomanov (1997)	Cogley (1998)
Runoff (km^3)		37,713	42,648	42,353

The terrestrial area is defined as the common denominator of the model-specific land masks from LPJ, WBM, WaterGAP, and Macro-PDM ($\sim 131 \times 10^6$ km^2). The data of Baumgartner and Reichel (1975), Shiklomanov (1997) both are based on an area sized $\sim 135 \times 10^6$ km^2. The time period is 1961–1990 for the model results, and varies among basins and regions for Baumgartner and Reichel (1975), Shiklomanov (1997), and Cogley (1998).

Table 3
Measures of agreement between observed (Fekete et al., 1999) and simulated annual runoff (km^3)

All basins ($n = 663$)	LPJ	Model 1	Model 2	Model 3				
A	0.89	0.89	0.92	0.9				
B	−407	−1471	−386	442				
Basin	Amazon (Óbidos)	Danube (Leatal Izmail)	MacKenzie (Norman Wells)	Mississippi (Tarbert Landing)	Murray (Lock 9 Upper)	Nile (El Ekhsase)	Yenisei (Igarka)	Zaire (Kinshasa)
n (years)[a]	32	60	19	16	16	12	49	59
A	0.43	0.82	0.47	0.55	0.12	0.01	0.26	0.47
B	999	−17	−78	194	77	470	−220	193

Upper panel: long-term means (1961–1990) computed by LPJ and the three hydrological models for 663 basins (various time periods). Lower panel: LPJ simulations for a selection of large rivers. See Section 3 for definition of the index of agreement (*A*), and the mean bias error (*B*).

[a] The respective time periods are indicated in Fig. 6.

the Amazon and the Zaire is also well captured, it is underestimated for the MacKenzie and the Yenisei. Particularly, the spring peak of the latter is computed too low. In contrast, LPJ simulates too high runoff for rivers crossing semi-arid and arid regions, such as the Nile and the Murray (Figs. 5 and 6; Table 3).

The overall nature and magnitude of the simulation biases, and the hydro-climatic zones in which they occur, are in agreement with findings from other macro-scale models (e.g. Fekete et al., 2002; Fig. 3 in Döll et al., 2003; Fig. 4). This evidence suggests that the relevant reasons for biases in our runoff estimates are common to large-scale models, i.e. they are not specific to LPJ. For example, much of the overestimation for Africa (Fig. 4) is due to the significant bias for sub-Saharan rivers such as the Niger and the Senegal (Fig. 2c) and, particularly, for the Nile (Fig. 5). These deviations, however, are not surprising, as the modelled hydrographs clearly follow the seasonal distribution of precipitation (Fig. 6), although in reality the relationship between basin-wide rainfall and runoff is not straightforward in these regions (e.g. Conway and Hulme, 1993). The influence of precipitation on those rivers' downstream runoff is masked by a variety of other processes, such as evaporation loss from lakes, reservoirs, wetlands, non-perennial ponds and from the river channel; flood plain–channel interactions; seepage into groundwater; inter-basin transfers; and human water withdrawal (Kite, 1998). These processes are not yet accounted for explicitly in global vegetation models such as LPJ. However, global hydrology models also tend to overestimate runoff in arid regions (see Africa and Australia in Fig. 4), owing to inadequate representation of these processes (Döll et al., 2003).

The poor seasonal performance of all four models in South America (Fig. 4) can be seen in their failure to reproduce the Amazon's runoff. The LPJ-simulated hydrograph of this stream follows the seasonal course of precipitation, which leads to a pronounced mismatch in the timing of calculated monthly runoff generation and observed discharge at the gauge, Óbidos (Fig. 6). This time-lag is due to the model's lack of a river routing scheme: simple addition of daily runoff from each grid cell within a river's basin unrealistically reaches the river mouth that day. Similar problems are inherent in other models that do not consider river routing (e.g. Nijssen et al., 2001). However, even WaterGAP and WBM—which include a simple routing component—also do not capture sufficiently the seasonal dynamics of runoff and retention within the Amazon basin (Fig. 4), since the low flow velocity of this stream requires additional model tuning (Döll et al., 2003). Moreover, sparseness of precipitation data, and possibly poor representation of precipitation distribution in mountainous regions, contribute notably to the general poor performance in this region (Fekete et al., 1999). The fact that neighbouring basins in this region are either over- or underestimated by LPJ (Fig. 2c) may reflect such uncertainties in the underlying precipitation data.

The rather low runoff computed for many northern high-latitude rivers such as the MacKenzie and the Yenisei (Figs. 2c and 5) is also not specific to LPJ, yet well-known from other macro-scale models (Fekete

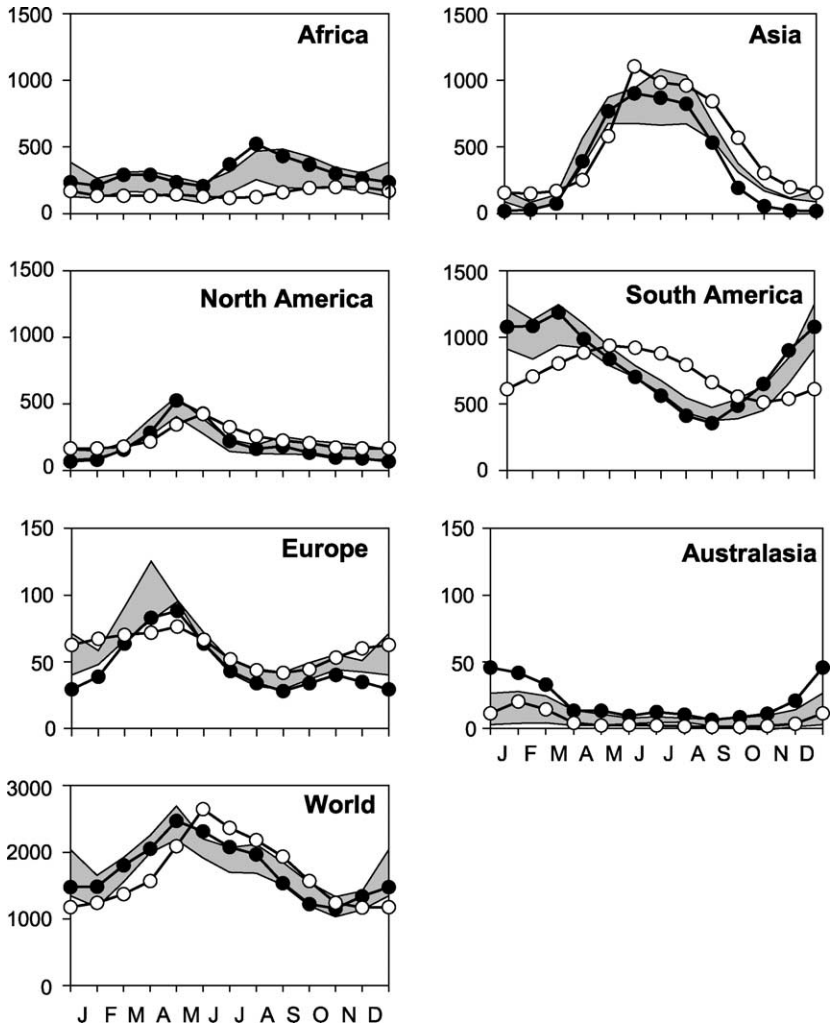

Fig. 4. Long-term (1961–1990) monthly means of runoff (km^3) for observed parts of the continents (cf. Fig. 2c), simulated by LPJ (filled symbols) and the three global hydrological models (range indicated by shaded area). The observations (open symbols) are taken from Fekete et al. (1999).

et al., 1999; Döll et al., 2003; Fig. 4). Again, biased estimates of precipitation contribute to the overall underestimation in these snow-dominated regions. The simulated early runoff (Fig. 6) is likely due to the fact that river routing and retention by wetlands and lakes are not considered in DGVMs such as LPJ. The tendency towards zero runoff in winter, and the high-magnitude of the spring peak (both of which are also obvious for the Danube) are probably related to the linear interpolation of monthly air temperature to daily values, and to the simplified representation of snow formation and melt (Eq. (12)). This approach neglects short-term snow melt events, and may lead to an overestimation of accumulated snowpack; Döll et al. (2003) documented similar problems with WaterGAP. Moreover, LPJ currently does not consider permafrost, which exerts significant influences on both the magnitude and the timing of runoff generation.

One might expect that DGVMs should perform worse than other models in agricultural regions, because they consider natural vegetation only, thereby

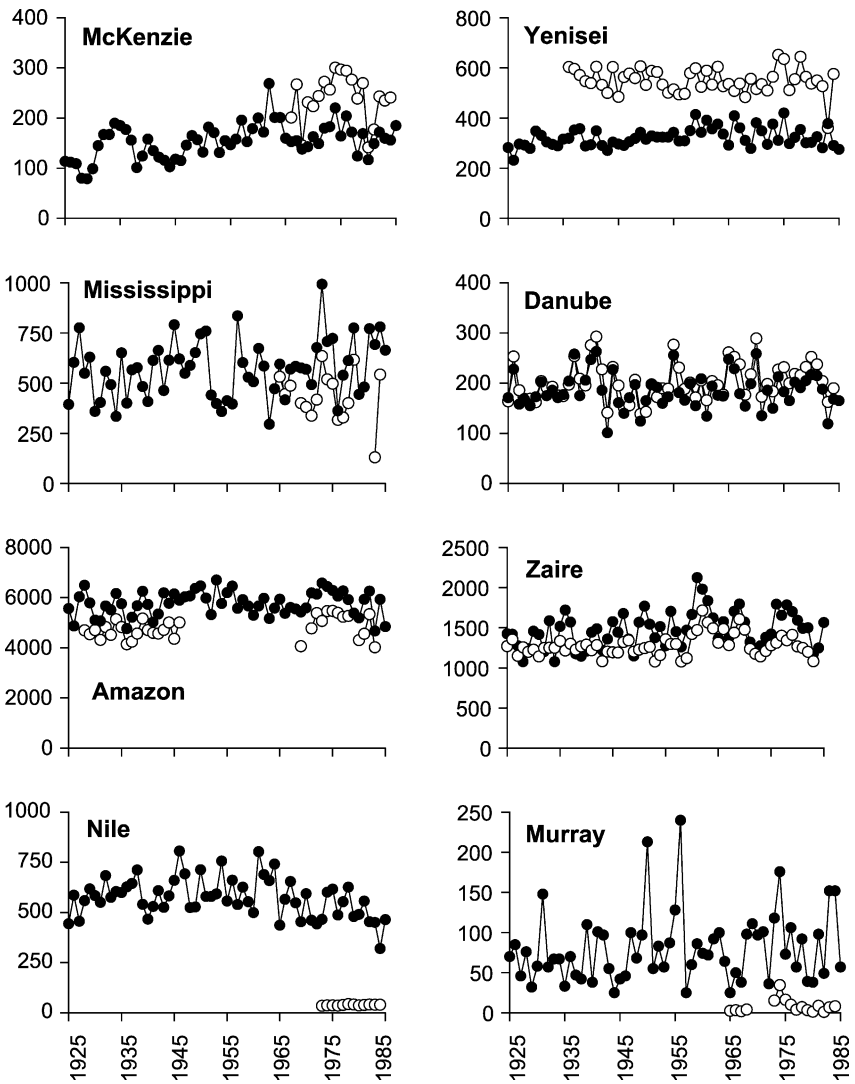

Fig. 5. Time series of observed (open symbols) and simulated (filled symbols) annual runoff (km^3) from selected river basins. The observations are taken from Vörösmarty et al. (1996) and represent discharge at the basin outlets. The simulated values are area-weighted sums of runoff from all grid cells within the basin boundaries.

ignoring human land-use conversions (crop cultivation, deforestation, etc.). These impacts are pervasive; Ramankutty and Foley (1998) suggest that about 18 million km^2 of the land surface are currently under cultivation. Consequently, simulated runoff should be too low in regions where the model diagnoses a dominance of woody PFTs, although cropland actually dominates. The tendency towards low runoff estimates (especially during the summer season) across parts of Europe and North America (Fig. 4) may be related to the missing representation of cropland. To test this hypothesis, we compared simulated and observed runoff for 41 European basins where agricultural land use predominates, and for another 23 ›undisturbed‹ basins (runoff data from Fekete et al., 1999). Grid cells were classified as cropland based on a MODIS global land cover data set for 2000/2001 (Friedl et al., 2002). Basins were

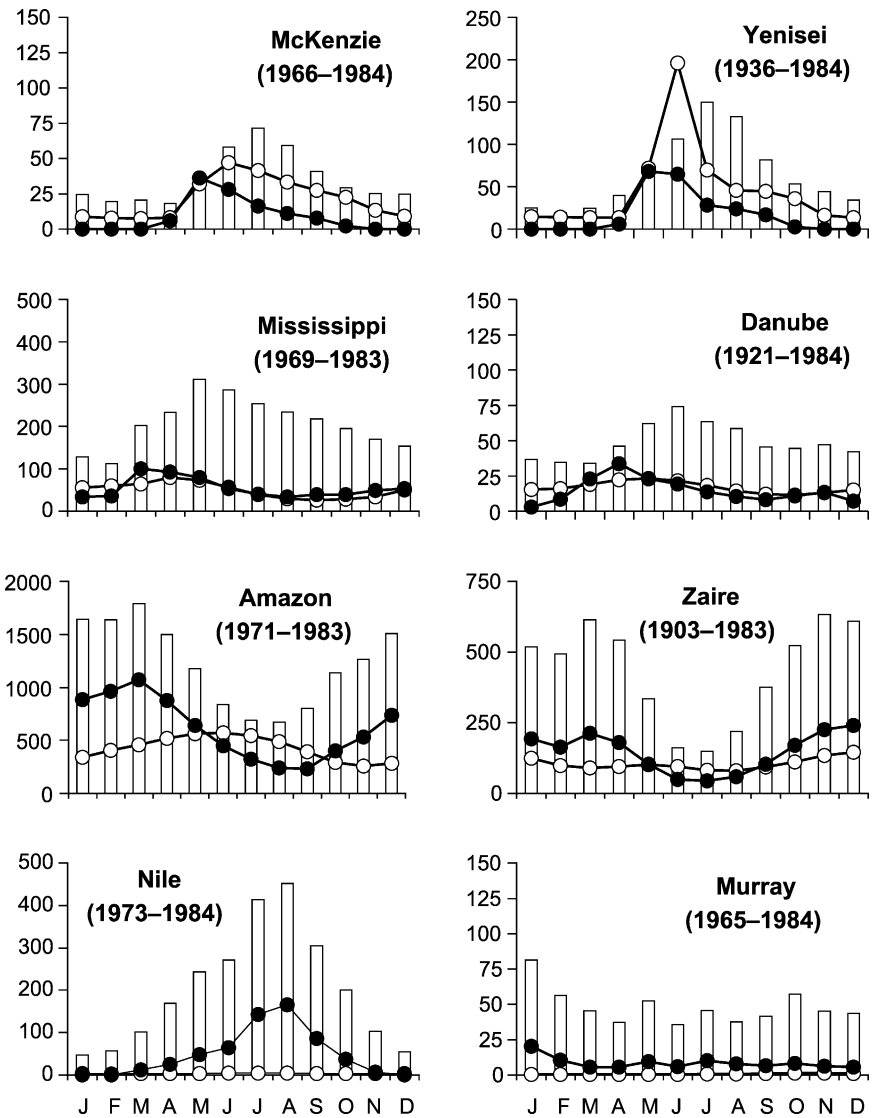

Fig. 6. Long-term monthly means (km^3) of observed (open symbols) and simulated runoff (filled symbols) for a selection of large river basins. The bars represent area-weighted monthly means (km^3) of precipitation from the CRU05 data set (New et al., 2000). Details as in Fig. 5.

considered as dominated by cropland if >80% of all grid cells within the catchment area each contain >50% crops according to the MODIS data. Analysis was focused on Europe, since impacts of water consumption and irrigation are weak there compared to, for example, the US and Southeast Asia (Döll and Siebert, 2002). It was found that the underestimation of simulated runoff is in fact most pronounced in those basins where agricultural land use dominates ($B = -36.7$; $A = 0.79$), while there is very good agreement for woodlands ($B = 1.9$; $A = 0.86$) (Fig. 8). To assess whether consideration of cropland would improve the simulation results, we forced the model to suppress growth of trees in the cropland-dominated areas, such that only grasses were allowed to establish. As a result, simulation quality for these basins was indeed improved considerably ($A = 0.92$). Analysis of monthly results (data not shown) revealed

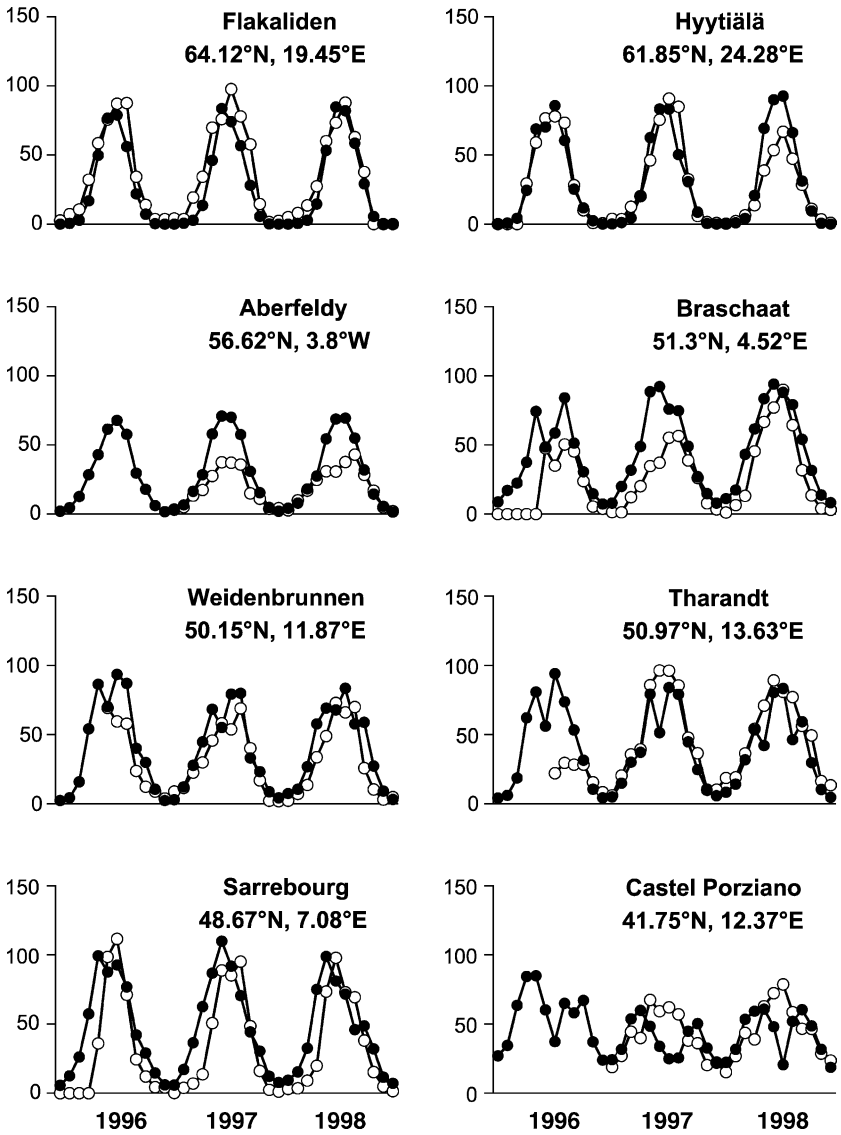

Fig. 7. Measured (open symbols) and simulated (filled symbols) monthly evapotranspiration (mm) for diverse European forests (EUROFLUX sites, 1996–1998). The observed values are scaled by a factor of 1.2 to account for measurement imbalance (see text).

that the underestimation in summer runoff across the continent (Fig. 4) becomes negligible when grassland is introduced. However, runoff is still underestimated in winter, and, as a consequence, annual totals remain somewhat too low ($B = -31.0$). This bias is likely related to the above-described problems in snow modelling, and to the fact that delayed runoff from groundwater reservoirs is not considered in the model.

5. Results of the 2 × CO_2 simulation experiment

Fig. 9 shows regions with statistically significant changes in runoff and evapotranspiration predicted under a hypothetic doubling of atmospheric CO_2 content (period 1961–1990). Runoff increases significantly ($p < 0.05$) under this scenario in the northernmost latitudes, and in the wet tropics. In contrast, it decreases particularly in subtropical

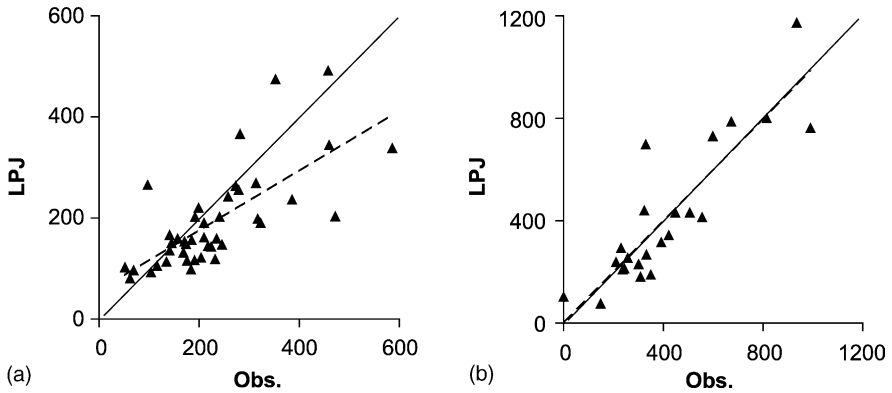

Fig. 8. Scatterplot of observed vs. simulated runoff ($km^3\ year^{-1}$) for European river basins dominated by (a) cropland ($n = 42$) and (b) woodland ($n = 23$). The diagonal lines refer to a 1:1 ratio of simulated and observed values; the dashed lines represent a linear regression curve. Note that the time periods vary among basins (Fekete et al., 1999).

regions (Fig. 9a). These changes in runoff generation are mainly related to concurrent changes in plant transpiration (Fig. 9b). While a significant decrease in transpiration occurs in large parts of the world, it is most pronounced in inner-tropical regions (up to 170 mm $year^{-1}$ in Central Africa). The overall decrease in transpiration reflects an increased carbon assimilation rate and an associated decrease in water loss through the stomata, which is a corollary of elevated CO_2. This effect is most pervasive in non-water limited environments such as the wet tropics (Fig. 9a), whereas in drier regions, water stress restricts transpiration irrespective of ambient CO_2 concentration (supply limitation, Eq. (5)). The lower transpiration results in increased evaporation (Fig. 9c), as there is more water stored in the soil column. The significant runoff increase in subpolar regions suggests that reduced transpiration cannot be compensated for by soil evaporation from the upper 20 cm (Eq. (9)). The runoff decrease in semi-arid regions (Fig. 9a) is obviously related to some expansion of forests into savannah and grassland into dry regions, owing to increased water use efficiency (Cramer et al., 2001). Accordingly, transpiration increases in these regions, whereas soil evaporation decreases (Fig. 9b and c). The generally higher interception loss (Fig. 9d) is probably attributable to an overall increase in net primary production and associated higher LAI (Eq. (2); Lockwood, 1999).

On balance, pronounced changes in the components of evapotranspiration would occur at doubled atmospheric CO_2 content. The net effect on runoff, however, is moderate (+5.5% change globally), although regional differences are prominent. These changes are driven by dynamics within the plant–water system, which are not accounted for in stand-alone hydrological models. For example, earlier studies with hydrological models likely overestimated effects of CO_2-induced vegetation changes on the water balance, due to a number of simplifying assumptions (Idso and Brazel, 1984; Kite, 1993). In particular, physiological changes in vegetation were emulated in these studies by only reducing evapotranspiration, while feedback mechanisms between vegetation and water cycling were omitted. Similarly to the present study, however, previous work based on equilibrium biogeography models also suggests moderate changes in evapotranspiration and runoff due to CO_2- and climate-driven changes in stomatal conductance (physiological effect) and leaf area (structural effect). For instance, Neilson and Marks (1994) found an increase in global runoff by about 13% in response to doubled CO_2. The difference to our projections may stem from the fact that those authors used an earlier climatic database, and omitted effects of transient changes in vegetation structure and distribution, which can only be determined by dynamic vegetation models such as LPJ. Further evidence that our simulations are realistic is provided by Hickler et al. (2003), who found that effects of elevated CO_2 simulated by LPJ lie well within the range observed at the Duke Forest FACE (Free Air CO_2 Enrichment) experiment.

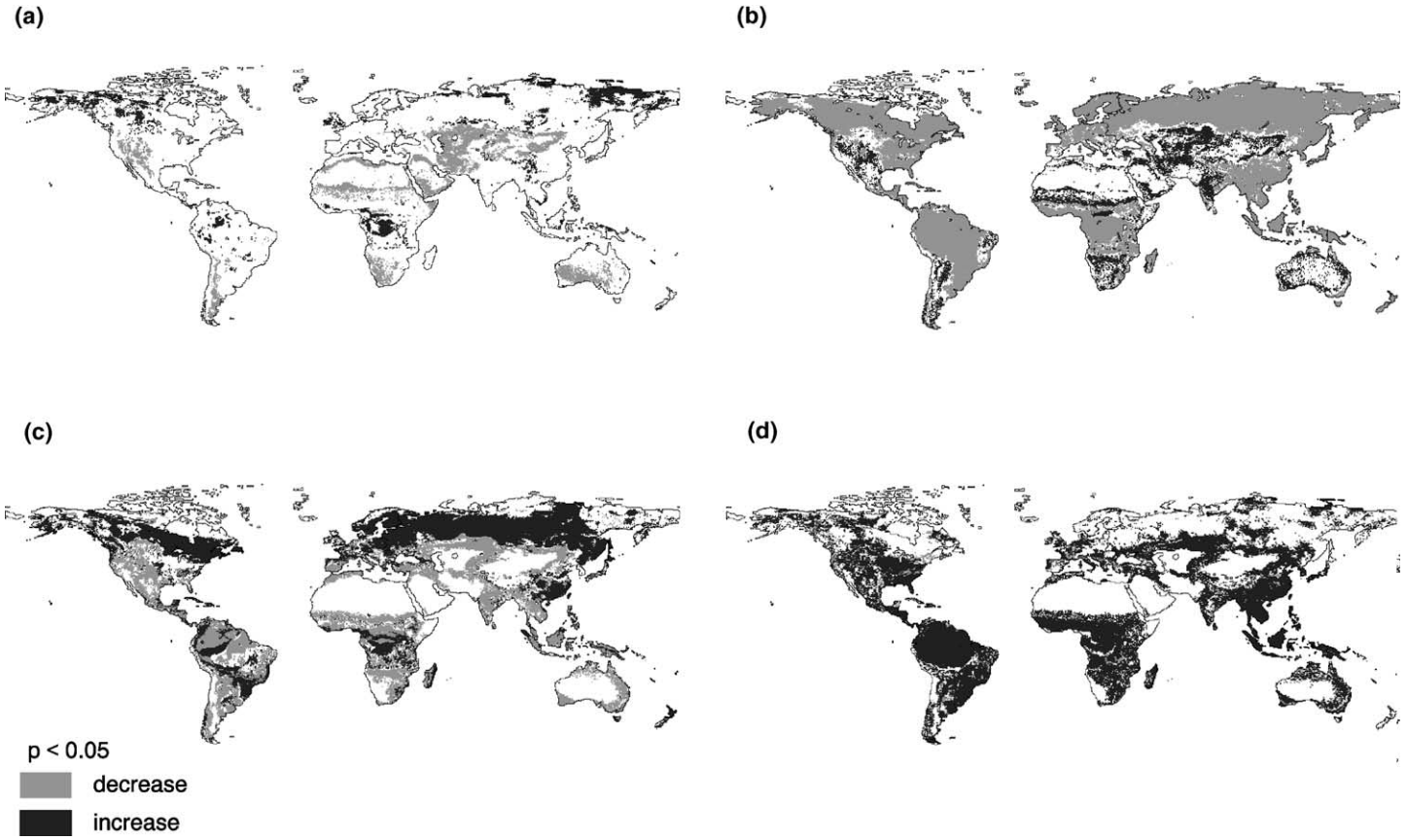

Fig. 9. Regions with significant changes in (a) runoff, (b) transpiration, (c) evaporation from bare soil, and (d) interception under the CO_2-doubling scenario. Light shading indicates significant decreases, dark shading indicates significant increases for 1961–1990, according to the Mann–Whitney test ($p < 0.05$).

6. Discussion and conclusions

Global hydrological models are essential tools for examining variations in water balance components on scales larger than regional (Arnell, 1999b; Alcamo et al., 2000; Vörösmarty et al., 2000; Döll et al., 2003). Although these models adequately represent most of the hydrological processes relevant at the macro-scale, they largely lack mechanistic links between the biosphere and the hydrosphere, such as the coupling of plant transpiration to atmospheric CO_2 content and related feedbacks to soil moisture and runoff generation. The simulation of dynamic interactions between terrestrial vegetation and water, however, is a crucial prerequisite for realistic assessment of past and future changes in large-scale water supply and demand. DGVMs are well suited tools for elucidating such biosphere–hydrosphere interrelations, given that the computed water balance is thoroughly validated. As documented here, the hydrological performance of LPJ, a well established model in this field, is largely similar to that of stand-alone global hydrological models. Moreover, the simulation experiment clearly demonstrated that dynamic modelling of the coupled terrestrial carbon and water cycle is not trivial, as it enables to quantify important processes that would be neglected otherwise. In fact, a doubling of atmospheric CO_2 content alone—performed for demonstrational purposes here, but highly relevant for future projections—resulted in significant changes in evapotranspiration and runoff around the world. The signature of these changes is strongly regional.

The overall correspondence among runoff simulations of LPJ and other models indicates that both macro-scale hydrology models and DGVMs are subject to the same major sources of uncertainty. Thus, we reinforce the hypothesis that the accuracy of modelled water budgets is considerably compromised by the quality and spatial resolution of climate input data (Arnell, 1999a; Fekete et al., 2002). Possible ways to deal with this problem are an overall correction for precipitation measurement errors (Arnell, 1999a), basin-specific corrections for precipitation biases (Fekete et al., 2002; Milly and Shmakin, 2002), or tuning of computed runoff (Döll et al., 2003). To avoid 'over-tuning', analysis may be restricted to those regions for which reliable precipitation records are available, or for which underlying uncertainties can be quantified (Milly and Dunne, 2002). Furthermore, uncertainties in the soil data, and the definition of only two soil layers with fixed thickness may bias LPJ-computed evapotranspiration and runoff. Therefore, it is planned to introduce additional soil layers, and to consider subgrid-scale variability of soil moisture as related to topography (e.g. Walko et al., 2000).

The general tendency towards early runoff in the LPJ simulations does not necessarily mean that the calculations are inaccurate. These biases are rather artefacts, because in the absence of river routing, simulated basin-wide runoff generation certainly cannot match discharge observed at the basin outlet. Implementation of a river routing scheme, consideration of water storage in lakes, reservoirs and wetlands, and better representation of snow storage and melt, will allow for direct comparison of simulated runoff and observed discharge. Moreover, preliminary simulations of the extent and seasonal variation of an active permafrost layer substantially improved runoff estimates for subarctic regions (Christian Beer, unpublished data). These model refinements are expected to generally improve the seasonal timing of runoff computed by the LPJ model (Coe, 2000; Oki et al., 2001). Additional improvement should be attained by explicit representation of evaporation from perennial and ephemeral water bodies. Refined parameterisation of vegetation responses to water stress (e.g. a PFT-specific supply approach, and the dynamic representation of rooting depths) will further improve the water balance computed by LPJ.

Given that runoff generation is simulated realistically, biogeochemical applications of DGVMs (assessments of carbon pools, biogeographical distribution of PFTs, etc.) should not be affected by the lack of a routing scheme and the missing representation of human water withdrawal from rivers and lakes. Once runoff has reached the river network, it is largely unavailable to terrestrial vegetation. However, reliable estimates of water transport among grid cells, as well as water storage and consumption within the cells, will be required if the model were to be applied as an integrated tool for assessing global freshwater supply and demand for human use (Döll et al., 2003). For instance, studies

of inter-dependencies between water availability and food requirements and their future changes rely on accurate estimates of downstream water transport, storage in lakes and reservoirs, and consumptive use for irrigation (Cai and Rosegrant, 2002; Döll and Siebert, 2002). Since such assessments also require consideration of cropland, a number of ›crop functional types‹, complementary to the PFTs, are currently being implemented into the LPJ model. This addition is expected to also eliminate the underestimation of runoff in agricultural regions, as discussed above.

The $2 \times CO_2$ simulation experiment demonstrates that the LPJ model is adequate to explore possible vegetation-driven changes in the terrestrial water balance in response to a warmer future climate. Analogously, reverse effects of changing hydrological conditions on vegetation and the carbon balance can be investigated. It has to be stressed, however, that feedbacks from the biosphere to the atmosphere are not considered in LPJ. For example, structural changes in vegetation may warm the land surface by lowering its albedo, or cool it by enhancing evapotranspiration (Betts et al., 1997). In turn, such effects would feed back to vegetation and the water cycle. Studies of complex atmosphere–biosphere interactions and their repercussions to land surface hydrology require fully coupled dynamic vegetation and climate models (Foley et al., 1998).

In summary, the capacity of the LPJ-DGVM to simulate the coupled terrestrial carbon and water cycle makes it a useful tool for examining ecohydrological processes at large scales. The importance of explicitly modelling plant–water relationships and their spatio-temporal dynamics was clearly demonstrated by the CO_2-doubling simulation experiment. DGVMs such as LPJ, hence, are poised to contribute essentially to the understanding of inter-dependencies between the terrestrial water budget and the world's major vegetation types at annual to centennial time scales.

Acknowledgements

The manuscript benefited from critical readings by and fruitful discussion with Franz-W. Badeck, Wolfgang Cramer, Valentina Krysanova, Colin Prentice, Benjamin Smith, and Michael Vohland. We are grateful to Nigel Arnell and Petra Döll for providing simulation results from their models. Almut Arneth is acknowledged for providing EUROFLUX data. The CRU05 climate data were supplied by the Climate Impacts LINK project on behalf of the Climatic Research Unit, University of East Anglia. This study was funded by the German Ministry for Education and Research under the German Climate Research Programme DEKLIM (project CVECA).

References

Alcamo, J., Henrichs, T., Rösch, T., 2000. World water in 2025—global modelling and scenario analysis for the World Commission on Water for the 21st Century. Kassel World Water Series 2, Center for Environmental Systems Research, University of Kassel, Germany.

Arnell, N.W., 1999a. A simple water balance model for the simulation of streamflow over a large geographic domain. J. Hydrol. 217, 314–335.

Arnell, N.W., 1999b. Climate change and global water resources. Glob. Environ. Change 9, S31–S49.

Arora, V., 2002. Modeling vegetation as a dynamic component in soil–vegetation–atmosphere transfer schemes and hydrological models. Rev. Geophys. 40, 3.1–3.26.

Baumgartner, A., Reichel, E., 1975. Die Weltwasserbilanz, R. Oldenbourg Verlag, Munich, Vienna.

Betts, R.A., Cox, P.M., Lee, S.E., Woodward, F.I., 1997. Contrasting physiological and structural vegetation feedbacks in climate change simulations. Nature 387, 796–799.

Bosch, J.M., Hewlett, J.D., 1982. A review of catchment experiments to determine the effect of vegetation changes on water yield and evapotranspiration. J. Hydrol. 55, 3–23.

Cai, X., Rosegrant, M.W., 2002. Global water demand and supply projections. Water Int. 27, 159–169.

Choudhury, B.J., DiGirolamo, N.E., Susskind, J., Darnell, W.L., Gupta, S.K., Asrar, G., 1998. A biophysical process-based estimate of global land surface evaporation using satellite and ancillary data—II. Regional and global patterns of seasonal and annual variations. J. Hydrol. 205, 186–204.

Churkina, G., Running, S.W., Schloss, A.L., The participants of the Potsdam NPP model intercomparison, 1999. Comparing global models of terrestrial net primary productivity (NPP): the importance of water availability. Glob. Change Biol. 5 (Suppl. 1), 46–55.

Coe, M.T., 2000. Modeling terrestrial hydrological systems at the continental scale: testing the accuracy of an atmospheric GCM. J. Climate 13, 686–704.

Cogley, J.G., 1998. GGHYDRO—Global Hydrographic Data, Release 2.2. Trent Climate Note 98-1, Department of Geography, Trent University, Peterborough, Ont., Canada.

Conway, D., Hulme, M., 1993. Recent fluctuations in precipitation and runoff over the Nile sub-basins and their impact on main Nile discharge. Clim. Change 25, 127–151.

Cramer, W., Bondeau, A., Woodward, F.I., Prentice, I.C., Betts, R.A., Brovkin, V., Cox, P.M., Fisher, V., Foley, J., Friend, A.D., Kucharik, C., Lomas, M.R., Ramankutty, N., Sitch, S., Smith, B., White, A., Young-Molling, C., 2001. Global response of terrestrial ecosystem structure and function to CO_2 and climate change: results from six dynamic global vegetation models. Glob. Change Biol. 7, 357–373.

Döll, P., Siebert, S., 2002. Global modelling of irrigation water requirements. Water Resour. Res. 38, 1037–1046.

Döll, P., Kaspar, F., Lehner, B., 2003. A global hydrological model for deriving water availability indicators: model tuning and validation. J. Hydrol. 270, 105–134.

Dunn, S.M., Mackay, R., 1995. Spatial variation in evapotranspiration and the influence of land use on catchment hydrology. J. Hydrol. 171, 49–73.

Eamus, D., Jarvis, P.G., 1989. The direct effects of increase in the global atmospheric CO_2 concentration on natural and commercial temperate trees and forests. Adv. Ecol. Res. 19, 1–55.

Eckhardt, K., Breuer, L., Frede, H.G., 2003. Parameter uncertainty and the significance of simulated land use change effects. J. Hydrol. 273, 164–176.

Food and Agriculture Organization, 1991. The Digitized Soil Map of the World (Release 1.0), FAO, Rome.

Federer, C.A., 1982. Transpirational supply and demand: plant, soil, and atmospheric effects evaluated by simulation. Water Resour. Res. 18, 355–362.

Fekete, B.M., Vörösmarty, C.J., Grabs, W., 1999. Global composite runoff fields of observed river discharge and simulated water balances. Report No. 22, Global Runoff Data Centre, Koblenz.

Fekete, B.M., Vörösmarty, C.J., Grabs, W., 2002. High-resolution fields of global runoff combining observed river discharge and simulated water balances. Glob. Biogeochem. Cycles 16 doi: 10.1029/1999GB001254.

Foley, J.A., Prentice, I.C., Ramankutty, N., Levis, S., Pollard, D., Sitch, S., Haxeltine, A., 1996. An integrated biosphere model of land surface processes, terrestrial carbon balance, and vegetation dynamics. Glob. Biogeochem. Cycles 10, 603–628.

Foley, J.A., Levis, S., Prentice, I.C., Pollard, D., Thompson, S.L., 1998. Coupling dynamic models of climate and vegetation. Glob. Change Biol. 4, 561–579.

Foley, J.A., Botta, A., Coe, M.T., 2002. El Niño—Southern oscillation and the climate, ecosystems and rivers of Amazonia. Glob. Biogeochem. Cycles 16 doi: 10.1029/2002GB001872.

Friedl, M.A., McIver, D.K., Hodges, J.C., Zhang, X.Y., Muchoney, D., Strahler, A.H., Woodcock, C.E., Gopal, S., Schneider, A., Cooper, A., Bacinni, A., Gao, F., Schaaf, C, 2002. Global land cover mapping from MODIS: algorithms and early results. Remote Sensing Environ. 83, 287–302.

Geng, S., Penning de Vries, F.W.T., Supit, I., 1986. A simple method for generating daily rainfall data. Agric. Forest Meteorol. 36, 363–376.

Gitay, H., Brown, S., Easterling, W., Jallow, B., 2001. Ecosystems and their goods and services. In: McCarthy, J.J., Canziani, O.F., Leary, N.A., Dokken, D.J., White, K.S. (Eds.), Climate Change 2001: impacts, adaptation, and vulnerability, Contribution of Working Group II to the Third Assessment Report of the Intergovernmental Panel on Climate Change, Cambridge University Press, Cambridge, pp. 235–342.

Haxeltine, A., Prentice, I.C., 1996. BIOME3: an equilibrium terrestrial biosphere model based on ecophysiological constraints, resource availability, and competition among plant functional types. Glob. Biogeochem. Cycles 10, 693–709.

Henning, D., 1989. Atlas of the Surface Heat Balance of the Continents, Gebr. Borntraeger, Berlin, Stuttgart.

Hickler, T., Prentice, C., Smith, B., Sykes, M.T., 2003. Simulating the effects of elevated CO_2 on productivity at the Duke Forest FACE experiment: a test of the dynamic global vegetation model LPJ. Geophys. Res. Abstr. EGS-AGU-EUG Joint Assembly, Nice.

Hobbins, M.T., Ramírez, J.A., Brown, T.C., 2001. The complementary relationship in estimation of regional evapotranspiration: an enhanced advection-aridity model. Water Resour. Res. 37, 1389–1403.

Huang, J., van den Dool, H.M., Georgakakos, K.P., 1996. Analysis of model-calculated soil moisture over the United States, 1931–1993, and applications to long-range temperature forecasts. J. Climate 9, 1350–1362.

Huntingford, C., Monteith, J.L., 1998. The behaviour of a mixed-layer model of the convective boundary layer coupled to a big leaf model of surface energy partitioning, Bound-Lay. Meteorology 88, 87–101.

Hutjes, R.W.A., Kabat, P., Running, S.W., Shuttleworth, W.J., Field, C., Hoff, H., Jarvis, P.G., Kayane, I., Krenke, A.N., Liu, C., Meybeck, M., Nobre, C.A., Oyebande, L., Pitman, A., Pielke, R.A., Raupach, M., Saugier, B., Schulze, E.D., Sellers, P.J., Tenhunen, J.D., Valentini, R., Victoria, R.L., Vörösmarty, C.J., 1998. Biospheric aspects of the hydrological cycle. J. Hydrol. 212/213, 1–21.

Idso, S.B., Brazel, A.J., 1984. Rising atmospheric carbon dioxide concentrations may increase streamflow. Nature 312, 51–53.

Jackson, R.B., Canadell, J., Ehleringer, J.R., Mooney, H.A., Sala, O.E., Schulze, E.-D., 1996. A global analysis of root distributions for terrestrial biomes. Oecologia 108, 389–411.

Joos, F., Prentice, I.C., Sitch, S., Meyer, R., Hooss, G., Plattner, G.-K., Gerber, S., Hasselmann, K., 2001. Global warming feedbacks on terrestrial carbon uptake under the Intergovernmental Panel on Climate Change (IPCC) emission scenarios. Glob. Biogeochem. Cycles 15, 891–907.

Kelliher, F.M., Leuning, R., Schulze, E.-D., 1993. Evaporation and canopy characteristics of coniferous forests and grasslands. Oecologia 95, 153–163.

Kergoat, L., 1998. A model for hydrological equilibrium of leaf area index on a global scale. J. Hydrol. 212/213, 268–286.

Kimball, B.A., LaMorte, R.L., Pinter, P.J. Jr., Wall, G.W., Hunsaker, D.J., Adamsen, F.J., Leavitt, S.W., Thompson, T.L., Matthias, A.D., Brooks, T.J., 1999. Free-air CO_2-enrichment and soil nitrogen effects on energy balance and evapotranspiration of wheat. Water Resour. Res. 35, 1179–1190.

Kite, G.W., 1993. Application for a land class hydrological model to climate change. Water Resour. Res. 29, 2377–2384.

Kite, G., 1998. Land surface parameterizations of GCMs and macroscale hydrological models. J. Am. Water Resour. Assoc. 34, 1247–1254.

Korzun, V.I., Sokolov, A.A., Budyko, M.I., Voskrensensky, K.P., Kalinin, G.P., Konoplyantsev, A.A., Korotkevich, E.S., L'vovich, M.I., 1978. World Water Balance and Water Resources of the Earth, UNESCO Press, Paris.

Kucharik, C.J., Foley, J.A., Delire, C., Fisher, V.A., Coe, M.T., Lenters, J.D., Young-Molling, C., Ramankutty, N., 2000. Testing the performance of a dynamic global ecosystem model: water balance, carbon balance, and vegetation structure. Glob. Biogeochem. Cycles 14, 795–825.

Lenters, J.D., Coe, M.T., Foley, J.A., 2000. Surface water balance of the continental United States, 1963–1995: regional evaluation of a terrestrial biosphere model and the NCEP/NCAR reanalysis. J. Geophys. Res. 105 (D17), 22393–22425.

Levis, S., Coe, M.T., Foley, J.A., 1996. Hydrologic budget of a land surface model: a global application. J. Geophys. Res. 101 (D12), 16921–16930.

Lockwood, J.G., 1999. Is potential evapotranspiration and its relationship with actual evapotranspiration sensitive to elevated atmospheric CO_2 levels? Clim. Change 41, 193–212.

Loukas, A., Quick, M.C., 1999. The effect of climate change on floods in British Columbia. Nord. Hydrol. 30, 231–256.

Lucht, W., Prentice, I.C., Myneni, R.B., Sitch, S., Friedlingstein, P., Cramer, W., Bousquet, P., Buermann, W., Smith, B., 2002. Climatic control of the high-latitude vegetation greening trend and Pinatubo effect. Science 296, 1687–1689.

McGuire, A.D., Sitch, S., Clein, J.S., 2001. Carbon balance of the terrestrial biosphere in the twentieth century: analyses of CO_2, climate and land use effects with four process-based ecosystem models. Glob. Biogeochem. Cycles 15, 183–206.

Milly, P.C.D., 1997. Sensitivity of greenhouse summer dryness to changes in plant rooting characteristics. Geophys. Res. Lett. 24, 269–271.

Milly, P.C.D., Dunne, K.A., 2001. Macroscale water fluxes. 1. Quantifying errors in the estimation of basin mean precipitation. Water Resour. Res. 38 doi: 10.1029/2001WR000759.

Milly, P.C.D., Shmakin, A.B., 2002. Global modelling of land water and energy balances. Part II: land-characteristic contributions to spatial variability. J. Hydrometeor. 3, 301–310.

Monteith, J.L., 1995. Accommodation between transpiring vegetation and the convective boundary layer. J. Hydrol. 166, 251–263.

Neilson, R.P., 1995. A model for predicting continental-scale vegetation distribution and water balance. Ecol. Appl. 5, 362–386.

Neilson, R.P., Marks, D., 1994. A global perspective of regional vegetation and hydrologic sensitivities and risks from climatic change. J. Veget. Sci. 5, 715–730.

Neilson, R.P., Prentice, I.C., Smith, B., Kittel, T.G.F., Viner, D., 1998. Simulated changes in vegetation distribution under global warming. In: Watson, R.T., Zinyowera, M.C., Moss, R.H., Dokken, D.J. (Eds.), The Regional Impacts of Climate Change: An Assessment of Vulnerability, Cambridge University Press, Cambridge, pp. 439–456.

New, M., Hulme, M., Jones, P., 2000. Representing twentieth-century space-time climate variability. Part II: Development of 1901–1996 monthly grids of terrestrial surface climate. J. Clim. 13, 2217–2238.

Nijssen, B., O'Donnell, G.M., Lettenmaier, D., Lohmann, D., Wood, E.F., 2001. Predicting the discharge of global rivers. J. Clim. 14, 3307–3323.

Oki, T., Agata, Y., Kanae, S., Saruhashi, T., Yang, D., Musiake, K., 2001. Global assessment of current water resources using total runoff integrating pathways. Hydrol. Sci. J. 46, 983–995.

Peel, M.C., McMahon, T.A., Finlayson, B.L., Watson, F.G.R., 2001. Identification and explanation of continental differences in the variability of runoff. J. Hydrol. 250, 224–240.

Prentice, I.C., Sykes, M.T., Cramer, W., 1993. A simulation model for the transient effects of climate change on forest landscapes. Ecol. Model. 65, 51–70.

Prentice, I.C., Heimann, M., Sitch, S., 2000. The carbon balance of the terrestrial biosphere: ecosystem models and atmospheric observations. Ecol. Appl. 10, 1553–1573.

Priestley, C.H.B., Taylor, R.J., 1972. On the assessment of surface heat flux and evaporation using large-scale parameters. Mon. Weather Rev. 100, 81–92.

Ramankutty, N., Foley, J.A., 1998. Characterizing patterns of global land use: an analysis of global croplands data. Glob. Biogeochem. Cycles 12, 667–685.

Shiklomanov, I.A. (Ed.), 1997. Comprehensive Assessment of the Freshwater Resources of the World—Assessment of Water Resources and Water Availability in the World, WMO, Geneva.

Sitch, S., Smith, B., Prentice, I.C., Arneth, A., Bondeau, A., Cramer, W., Kaplan, J.O., Levis, S., Lucht, W., Sykes, M.T., Thonicke, K., Venevsky, S., 2003. Evaluation of ecosystem dynamics, plant geography and terrestrial carbon cycling in the LPJ dynamic global vegetation model. Glob. Change Biol. 9, 161–185.

Skiles, J.W., Hanson, J.D., 1994. Responses of arid and semiarid watersheds to increasing carbon dioxide and climate change as shown by simulation studies. Clim. Change 26, 377–397.

Stephenson, N.L., 1990. Climatic control of vegetation distribution: the role of the water balance. Am. Nat. 135, 649–670.

Valentini, R. (Ed.), 2003. Fluxes of Carbon, Water and Energy of European Forests, Springer, Heidelberg, 260 pp.

Venevsky, S., Thonicke, K., Sitch, S., Cramer, W., 2002. Simulating fire regimes in human-dominated ecosystems: Iberian Peninsula case study. Glob. Change Biol. 8, 984–998.

Vörösmarty, C.J., Fekete, B., Tucker, B.A., 1996. River Discharge Database, Version 1.0 (RivDIS v1.0). A contribution to IHP-V Theme 1. Technical Documents in Hydrology Series, UNESCO Press, Paris.

Vörösmarty, C.J., Federer, C.A., Schloss, A., 1998. Potential evaporation functions compared on US watersheds: implications for global-scale water balance and terrestrial ecosystem modelling. J. Hydrol. 207, 147–169.

Vörösmarty, C.J., Green, P., Salisbury, J., Lammers, R.B., 2000. Global water resources: vulnerability from climate change and population growth. Science 289, 284–288.

Wagner, W., Scipal, K., Pathe, C., Gerten, D., Lucht, W., Rudolf, B., 2003. A comparison of global remotely sensed soil moisture data with model and rainfall data. J. Geophys. Res. 108, D19, 4611, doi: 10.1029/2003JD003663.

Walko, R.L., Band, L.E., Baron, J., Kittel, T.G.F., Lammers, R., Lee, T.J., Ojima, D., Pielke, R.A. Sr., Taylor, C., Tague, C.,

Tremback, C.J., Vidale, P.J., 2000. Coupled atmosphere–biophysics–hydrology models for environmental modelling. J. Appl. Meteorol. 39, 931–944.

Wigley, T.M.L., Jones, P.D., 1985. Influences of precipitation changes and direct CO_2 effects on streamflow. Nature 314, 149–152.

Willmott, C.J., 1982. Some comments on the evaluation of model performance. Bull. Am. Meteor. Soc. 63, 1309–1313.

Wilson, K., Goldstein, A., Falge, E., Aubinet, M., Baldocchi, D., Berbigier, P., Bernhofer, C., Ceulemans, R., Dolman, H., Field, C., Grelle, A., Ibrom, A., Law, B.E., Kowalski, A., Meyers, T., Moncrieff, J., Monson, R., Oechel, W., Tenhunen, J., Valentini, R., Verma, S., 2002. Energy balance closure at FLUXNET sites. Agric. Forest Meteor. 113, 223–243.

Zobler, L., 1986. A world soil file for global climate modelling. NASA Tech. Memorandum, 87802.